Applied Catalysis B: Environmental 144 (2014) 792–799

Contents lists available at ScienceDirect

Applied Catalysis B: Environmental

journal homepage: www.elsevier.com/locate/apcatb

Effect of iron precursor on the Fenton-like activity of Fe_2O_3/mesoporous silica catalysts prepared under mild conditions

Jakelyne V. Coelho[a], Marina S. Guedes[a], Roberta G. Prado[a], Jairo Tronto[b], José D. Ardisson[c], Márcio C. Pereira[d], Luiz C.A. Oliveira[a,*]

[a] Departamento de Química, Universidade Federal de Minas Gerais, 31270-901 Belo Horizonte, Minas Gerais, Brazil
[b] Universidade Federal de Viçosa, Campus de Rio Paranaíba, Rodovia BR 354, km 310, 38810-000 Rio Paranaíba, Minas Gerais, Brazil
[c] Centro de Desenvolvimento da Tecnologia Nuclear, 31270-901 Belo Horizonte, Minas Gerais, Brazil
[d] Instituto de Ciência, Engenharia e Tecnologia,Universidade Federal dos Vales do Jequitinhonha e Mucuri, 39803-371 Teófilo Otoni, Minas Gerais, Brazil

ARTICLE INFO

Article history:
Received 18 April 2013
Received in revised form 24 July 2013
Accepted 9 August 2013
Available online 24 August 2013

Keywords:
Silica nanoparticles
Oxidation
Catalyst
Synthesis
Mesoporous

ABSTRACT

Fe_2O_3/mesoporous silica catalysts were prepared by adding Fe^{2+} or Fe^{3+} ions, as an iron precursor, during the synthesis of silica gel. Low angle XRD data showed that both iron precursors affected the hexagonal ordered arrays of silica, which were more perturbed by Fe^{2+} than by Fe^{3+} ions, as confirmed by TEM images. Based on the Mössbauer spectroscopy, XPS, EPR and NH_3-TPD data was possible to identify the iron species supported on the silica matrix are constituted of hematite and maghemite. The iron precursor strongly changed the specific area of the materials from 1406 $m^2\ g^{-1}$, in pure silica sample, to 1165 and 799 $m^2\ g^{-1}$ for the Fe3-MS and Fe2-MS samples, respectively, but the pore size distribution was maintained in the range of 15–40 Å in both samples. These Fe-containing silica nanoparticles showed good catalytic activity to degrade methylene blue in aqueous medium. However, the Fe3-MS sample was more active than the Fe2-MS sample because the iron in the first is more exposed, which facilitated the accessibility to the active Fenton-like sites. These synthesized samples showed to be more stable against the Fe leaching than samples prepared by simple impregnation of hematite on the silica surface. This was because the strong interaction of iron and silica matrix was achieved by adding iron in the course of the synthesis of silica gel.

1. Introduction

The development of new materials with higher pollutant removal capacity and reuse ability has contributed significantly to the treatment of contaminated effluents [1–3]. Silica nanoparticles (SNPs) with mesoporous channels between 2.5 and 10 nm in diameter are interesting materials to be used in heterogeneous catalysis because of their extraordinary textural characteristics such as high pore volume, tunable and uniform pore sizes and high specific area (>800 $m^2\ g^{-1}$) [4]. However, the catalytic uses of pure silica are limited.

In order to improve the catalytic activity of pure mesoporous SNPs for practical uses two main approaches have been used: (i) by substitution of structural Si by other metal cations such as Zr [5], Ti [6], Mn [7], Al [8], V [9], Zn [10], Ni [11], W [12] and Fe [13] or (ii) by impregnation of metal oxides such as Al_2O_3 [14], TiO_2 [15], Nb_2O_5 [16], Fe_2O_3 [17], etc. onto the silica extraframework. Among these transition metals, iron is a very promising material to be supported onto the silica extraframework or used as a dopant ion in the silica framework because of its catalytic properties and high availability on the Earth.

Mesoporous silica modified with Fe has been widely used as a catalyst in several reactions such as alkylation [18,19], isomerization [20], and in oxidation reactions to degrade different organic contaminant compounds in water [21–23]. Recently, Huang et al. [22] prepared Fe_2O_3 loaded mesoporous silica by hydrothermal and dipping method with good catalytic activity to oxidize *p*-chlorobenzoic acid by ozonation. Mesoporous silica with high iron content (Si/Fe = 20) was synthesized via the hydrothermal method by using Fe(III) oxalate as iron precursor, and it exhibited high oxidant efficiency to degrade phenol [23]. Maghemite/silica core–shell nanoparticles prepared by coating the surface of the magnetic core with silica by a nano-assembling method exhibited good Fenton-like activity to degrade phenol [24]. Choi et al. [25] reported the use of highly ordered iron-containing mesoporous silica, with 0.5–4 Fe/Si mol% loading, which exhibited high catalytic activity in phenol hydroxylation using H_2O_2 as oxidant. Both tetrahedral and octahedral iron was present in the composite, indicative of Fe in the silica framework and extraframework. Fe_2O_3/mesoporous silica (iron content = 1–11 wt.%) were prepared by adding iron nitrate

* Corresponding author. Tel.: +55 31 34096384; fax: +55 31 34095700.
E-mail address: luizoliveira@qui.ufmg.br (L.C.A. Oliveira).

0926-3373/$ – see front matter © 2013 Elsevier B.V. All rights reserved.
http://dx.doi.org/10.1016/j.apcatb.2013.08.022

in the course of MCM-41 synthesis or by impregnating iron nitrate or triiron oxoacetate complex on MCM-41. At room temperature, the Fe^{3+} ions leached from the silica matrix catalyzed the oxidation of phenol, while at 80 °C the oxidation of phenol occurred via a heterogeneous mechanism mediated by Fe^{3+} in the silica framework [26].

Ursachi et al. [27] reported that Fe_2O_3 can be stabilized inside the pore system of mesoporous silica. The ultrasound-assisted Fenton-like oxidation of methylene blue (100 mL, 0.03 mM, pH 3) in presence of the Fe_2O_3/silica catalysts (0.1 g) and 0.4 mL H_2O_2 (30%, w/w) removed about 96% of the initial quantity of MB within 60 min of reaction. Lam and Hu [28] showed that Fe/mesoporous silica can be prepared by using ferric acetylacetonate ($Fe(acac)_3$) as iron precursor. The prepared material showed good mineralization of orange II (85%) by the photo-Fenton process and low iron leaching concentration (~0.17 mg L^{-1}). Nanosized Fe_2O_3 loaded on mesoporous silica exhibited high photocatalytic degradation of indigo carmine dye in the presence of UV light (high pressure mercury lamp, 125 W, $\lambda < 365$ nm) [29].

Although the synthesis of Fe-containing mesoporous silica is widely reported in the literature, its catalytic activity strongly depends on the iron precursor and its preparation method, since iron can be only impregnated on the silica gel or added in the course of silica synthesis.

Herein, we reported the developing of a Fenton-like catalysts based on nanosized α-Fe_2O_3 impregnated on the mesoporous silica obtained by two different routes: (i) by adding iron(III) chloride or (ii) by adding iron(II) chloride in the course of the silica gel formation under mild synthesis conditions. The effect of an iron precursor on the catalytic properties of the synthesized materials was evaluated during the oxidation of methylene blue, a model molecule, using hydrogen peroxide as oxidant.

To the best of our knowledge most studies in the literature on the preparation of Fe_2O_3/mesoporous silica report the use of iron(III) precursor, i.e. iron(III) nitrate, iron(III) complexes, etc., during the silica gel formation. This is the first study on the effect of iron(II) precursor on the catalytic properties of α-Fe_2O_3/mesoporous silica.

2. Experimental

2.1. Catalysts synthesis

Mesoporous silica nanoparticles were synthesized by dissolving cetyltrimethylammonium bromide (CTAB) (1.63 g, 4.47 mmol, Vetec) in a mixture of 30 g of deionized water and 10 mL of 1 M NaOH solution, followed by the addition of TEOS (3.70 mL, 17.00 mmol, Aldrich) under stirring at 25 °C during 24 h at pH 11. After this time period, the pH of the suspension was adjusted to 7 by the addition of 1 M hydrochloric acid. The white precipitates were collected by centrifugation, washed with deionized water and dried at room temperature in a desiccator. To remove the surfactant, the solid materials were calcined in an electric furnace at 600 °C for 5 h under air flow (100 mL min^{-1}). This sample was labeled MS.

The mesoporous α-Fe_2O_3/silica nanoparticles were obtained by the same procedure described for the synthesis of pure silica, except for the addition, during the silica gel, of (i) 0.12 g (0.6 mmol) $FeCl_2 \cdot 4H_2O$ to a mixture of CTAB, water, NaOH and TEOS; this sample was labeled Fe2-MS and (ii) 0.16 g (0.6 mmol) $FeCl_3 \cdot 6H_2O$ to a mixture of CTAB, water, NaOH and TEOS; this sample was labeled Fe3-MS.

2.2. Characterization

The catalysts were characterized by nitrogen adsorption (−196 °C) in an AUTOSORB 1-Quantachrome system. The surface area was calculated using the BET model; the total pore volume was estimated from the amount of nitrogen adsorbed at $P/P_0 = 0.95$; and the pore size distribution was calculated based on the BJH theory. Energy dispersive X-ray spectroscopy (EDS) data were collected using an EDS/INCA 350 equipment. Mössbauer spectra were collected in constant acceleration transmission mode with a 10 mCi ^{57}Co/Rh source at 20 and 298 K. The data were stored in a 1024-channel MCS memory unit and were fitted using Lorentzian line shapes with a least-squares fitting procedure using the NORMOS program. Isomer shifts were calculated relatively to α-Fe. The content of Fe in the samples was determined by atomic absorption analyses on a Carl Zeiss Jena AAS instrument equipped with a background corrector for Zeeman polarization. TPD-NH_3 profiles were obtained with a Chembet-3000 (Quantachrome) equipped with a TCD detector. 0.2 g each catalyst was previously treated at 400 °C during 50 min under helium flow (80 mL min^{-1}) before adsorption of NH_3 at 50 °C. Then, the TPD-NH_3 profiles were collected at a heating rate of 10°/min up to 500 °C. The EPR spectra were recorded at room temperature with a custom-built X-band spectrometer (9.38 GHz) using a commercial cylindrical cavity (Bruker), a klystron (Varian) and an electromagnetic (Varian) with a maximum field amplitude of 800 mT. For the g factor calibration, 2,2-diphenil-2-picryhydrazyl (DPPH) was used as the standard ($g = 2.0037$). Transmission electron microscopy (TEM) images of all samples were taken with a JEOL transmission electron microscope model JEM 2000EXII. Powder X-ray diffraction (XRD) measurements of the samples were carried out using CuKα radiation in the 2θ ranges of 1.0–5.0° (low angle) on a RIGAKU D-MAX 2200 X-ray diffractometer. XPS measurements were made using an AEI ES200B spectrometer with a base pressure of better than 10^{-9} Torr using MgK_α X-ray radiation. Spectra were recorded to achieve maximum instrument resolution (better than 0.8 eV). Binding energies were calibrated using O 1s from oxide in the samples taken as 529.9 eV. Surface charge of nanoparticles was judged by zeta potential measurement on a Malvern Zetasizer 2000 HS (Malvern, UK).

2.3. Catalytic tests

The oxidation of methylene blue (MB) dye (model molecule, 100 mg L^{-1}) with H_2O_2 (8 mM) at pH 6 (natural pH of MB solution), was carried out with a total volume of 10 mL, using 10 mg of catalyst. All chemical reactions were performed under magnetic stirring in a recirculating temperature controlled bath kept at 25 ± 1 °C. The reactions were monitored with UV–vis spectroscopy (Shimadzu UV 1601 PC) at 665 nm.

2.4. Electrospray ionization (ESI)-mass spectrometry (MS) and TGMS

To identify the intermediate chemical species of the methylene blue oxidation reaction, an ION-TRAP LCQFleet (ThermoScientific, San Jose, CA) was used in positive ion mode. The reaction samples were analyzed by introducing aliquots into the ESI source with a syringe pump at a flow rate of 15 L min^{-1}. Spectra were obtained as averages of 5 scans of 0.2 s each. Typical ESI conditions used a heated capillary temperature of 275 °C, sheath gas (N_2) at a flow rate of 15 U (ca. 4 L min^{-1}), a spray voltage of 2 kV, a capillary voltage and a tube lens offset voltage of 25 V. The TGMS analysis was performed in an STA 449 F3 Jupiter (Netzsch).

3. Results and discussion

3.1. Characterization of the catalysts

The low angle XRD patterns of pure silica (MS) and Fe-containing silica synthesized from different iron precursors are shown in Fig. 1.

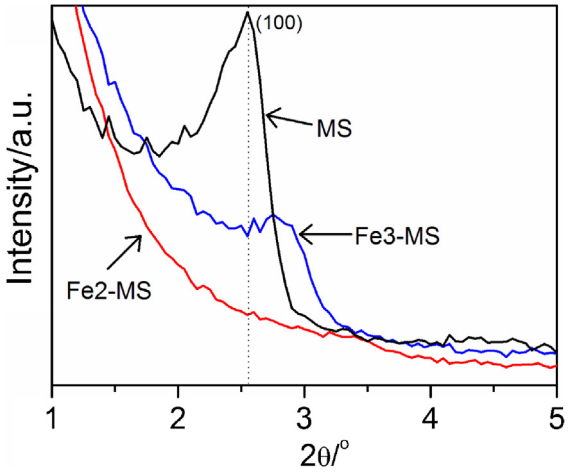

Fig. 1. Low angle XRD pattern of MS, Fe2-MS and Fe3-MS samples.

The diffraction peak (d_{100}) at around 2.5° 2θ in the low angle region of sample MS indicates the existence of some hexagonal order in the intra-particle mesoporous material. However, the absence of reflections relative to d_{110} and d_{200} suggests poor hexagonal geometry and periodicity of the mesoporous channels in the sample MS [30]. The XRD pattern of sample Fe3-MS revealed that the Fe^{3+} presence during the silica gel synthesis strongly affected the hexagonal symmetry of silica, as can be verified by the decreasing in the relative intensity of the d_{100} reflection as compared to the same peak in the sample MS. If Fe^{2+} ions were used as precursor (sample Fe2-MS) instead of Fe^{3+} no reflection could be observed in the XRD pattern at low angle, suggesting that the Fe^{2+} ions caused a collapse of the hexagonally ordered silica structure.

The total Fe_2O_3 content in the samples Fe2-MS and Fe3-MS was 5 wt.% and 5.9 wt.%, respectively. In order to determine how the iron species are located in the Fe-containing silica samples, ^{57}Fe Mössbauer measurements at 298 K were carried out. The fit of the Mössbauer spectra (Fig. 2) revealed that the iron in both samples is, as expected, only in the 3+ oxidation state, because any Fe^{2+} present in the samples can be easily oxidized to Fe^{3+} in air atmosphere, mainly at high temperatures as that used in this work. Mössbauer spectrum of Fe2-MS (Fig. 2) was fitted with one distribution model (sextets) due to non-homogeneous distribution of iron oxides over silica particles. The maximum hyperfine distribution field was 51.7 T, thus confirming the presence of hematite (δ = 0.36 mm s^{-1}, ε = −0.20 mm s^{-1}, relative subspectral area, RA = 60%) in the sample Fe2-MS. A smaller hyperfine field of 47.0 T (RA = 25%) also suggests the existence of maghemite in that sample. The others 15% (doublet, δ = 0.38 mm s^{-1}, Δ = 0.86 mm s^{-1}) are due to octahedral Fe^{3+} ions, likely finely divided Fe^{3+} oxides on the silica extraframework. No tetrahedral iron could be determined by Mössbauer spectroscopy, which suggests that iron in the sample Fe2-MS is present basically on the silica extraframework, as hematite or maghemite. The Mössbauer spectra of the sample Fe3-MS (Fig. 2a) showed the iron is located basically on the extraframework of silica. The two sextets, one corresponding to 36% (δ = 0.36 mm s^{-1}, B_{hf} = 49.5 T) and the other to 13% (δ = 0.37 mm s^{-1}, B_{hf} = 51.7 T) of the total iron, are respectively due to maghemite and hematite nanoparticles supported on the silica extraframework. Others 51% of relative area of the total iron (doublet, δ = 0.36 mm s^{-1}, Δ = 0.86 mm s^{-1}) correspond to smaller clusters of Fe^{3+} oxides nanoparticles embedded into the flexible pore walls of the mesoporous silica.

To better understand the origin for the presence of central doublet in samples Fe2-MS and Fe3-MS, Mössbauer spectra were also collected at 20 K (Fig. 2b). The results showed in both samples the presence of small clusters of maghemite and hematite.

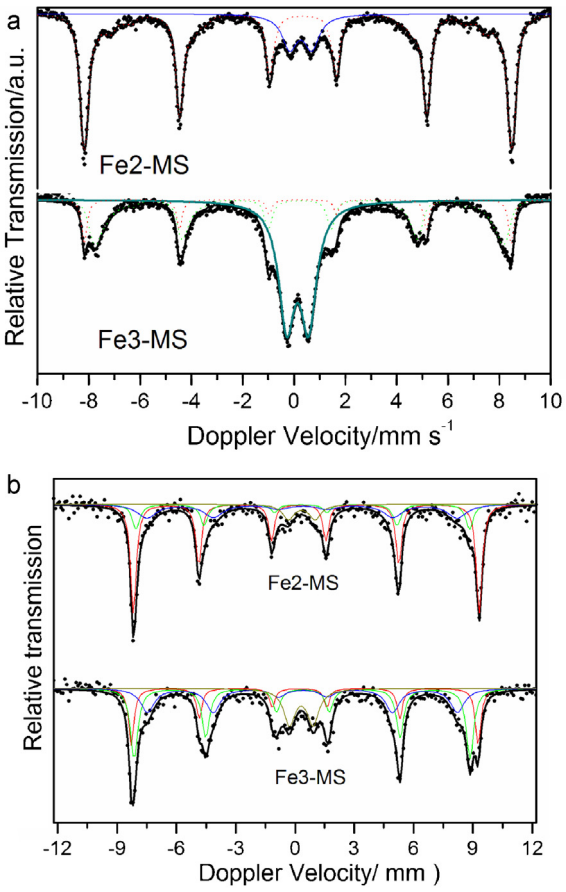

Fig. 2. Mössbauer spectroscopy of Fe2-MS and Fe3-MS samples collected at (a) 298 K and (b) 20 K.

Sample Fe2-MS was fitted with one Fe^{3+} sextet corresponding to hematite (RA = 51%), which underwent Morin Transition (δ = 0.48 mm s^{-1}, ε = 0.38 mm s^{-1} and B_{hf} = 54.2 T), two Fe^{3+} sextets due to maghemite; one of these sextets exhibited hyperfine field of 52.3 T (RA = 17%) and the another one showed smaller hyperfine field of 48.6 T (RA = 25%) due to the small size of these maghemite particles. In addition, 7% of the total spectra was due to Fe^{3+} (δ = .46 mm s^{-1}, Δ = 1.37 mm s^{-1}) octahedrally coordinated in the oxide structure. Sample Fe3-MS exhibited the same hyperfine parameters, but the relative subspectral area for hematite (B_{hf} = 54.2 T), maghemite (B_{hf} = 52.3 T), maghemite (B_{hf} = 48.6T) and Fe^{3+} doublet (δ = 0.46 mm s^{-1}, Δ = 1.37 mm s^{-1}) was 21, 38, 27 and 14%, respectively. The higher subspectral relative area for the Fe^{3+} doublet in sample Fe3-MS suggest that the iron in this sample is better dispersed on the silica matrix than in sample Fe2-MS.

The TEM images of MS, Fe2-MS and Fe3-MS samples are shown in Fig. 3. It can be clearly observed that sample MS (Fig. 3a and b) exhibited relatively well-ordered hexagonal array structures, as verified by the parallel fringes with narrow spacing along the pore direction. However, the Fe2-MS sample (Fig. 3c and d) does not exhibited any ordered arrays, indicating that the silica structure was collapsed due to the presence of Fe^{2+} during the silica gel synthesis. As verified by Mössbauer spectroscopy, the iron in this sample is in the form of hematite and maghemite, which was clearly visualized by the pseudo-spherical nanoparticles on the silica matrix shown in Fig. 3c. TEM images of sample Fe3-MS (Fig. 3e and f) showed that the some hexagonal arrays are maintained in the silica sample, however, they are not regularly ordered as in the SM sample. The iron oxides nanoparticles on the silica extraframework can also be clearly observable in Fig. 3e and f.

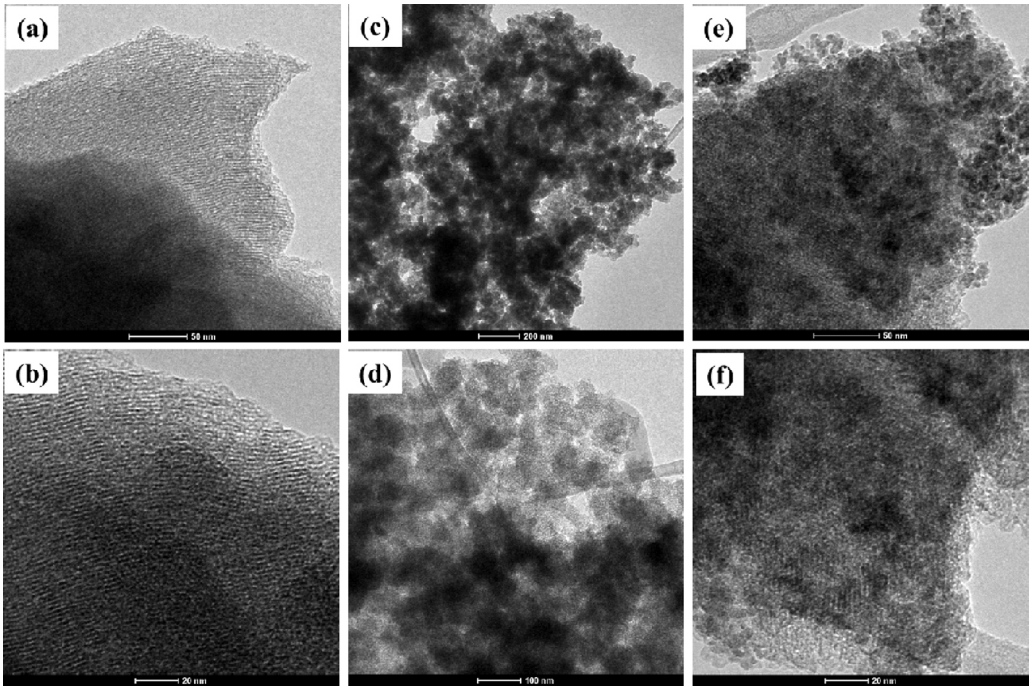

Fig. 3. TEM micrographs of samples (a and b) MS, (c and d) Fe2-MS and (e and f) Fe3-MS.

These iron oxides blocked the pore structure of silica as well as its orderliness.

The studied materials were also investigated by XPS in the region of Si 2p, Fe 2p and O 1s. The Si 2p spectra of all samples are shown in Fig. 4a. The spectrum of the MS sample was fitted with a single peak, centered at BE = 102.8 eV, which indicates only one type of surface electronic level such as Si—O bonding, in the silica structure. For the Fe2-MS and Fe3-MS samples a weak peak shifted to BE = 101.7 and 100.5 eV can be observed, respectively, suggesting strong interaction between the clusters of iron oxides and the silica matrix. Moreover, the Si 2p peak intensity for these samples decrease drastically with loading of iron on the silica extraframework, suggesting that Fe^{3+} oxide is covering the silica surface.

A very complex line-shape is observed in the Fe 2p spectra (Fig. 4b) of Fe2-MS and Fe3-MS samples. As expected, the MS sample does not show any signal, indicating the absence of iron in the silica surface. On the other hand, the spectra of Fe2-MS and Fe3-MS samples were fitted with six components. The peak at 710 eV in the sample Fe2-MS is assigned to Fe^{2+} $2p_{3/2}$, suggesting that this sample still has a small amount of Fe^{2+} on its surface, even after the thermal treatment in air atmosphere. Fe^{3+} oxides in this sample were determined from the strong peak at 720.1 eV ($Fe^{3+}_{sat.}$ $2p_{3/2}$) and 733.2 eV ($Fe^{3+}_{sat.}$ $2p_{1/2}$). The other peaks are due to shake-up satellites of the $2p_{3/2}$ and $2p_{1/2}$ peaks. In sample Fe3-MS the $Fe^{3+}_{sat.}$ $2p_{3/2}$ and $Fe^{3+}_{sat.}$ $2p_{1/2}$ peaks are shifted to 718.4 and 730.7 eV, respectively, due to the interaction between the clusters of iron oxides and the silica matrix.

The XPS spectra of O 1s are shown in Fig. 4c. The spectrum of sample MS is composed of a single peak centered at 533.1 eV due to the Si—O bonding. In the Fe2-MS and Fe3-MS samples this peak practically disappears, indicating that the silica matrix is covered by iron oxides nanoparticles. Moreover, this peak is shifted to 531.7 eV due to strong interaction between silica and Fe^{3+} oxides.

The NH_3-TPD curves for the synthesized materials are shown in Fig. 5. An increase in the ammonia desorption with the increase in the iron content can be clearly observed from Fig. 5. These data suggest that the sample Fe3-MS have higher amount of iron accessible to gaseous NH_3 than the sample Fe2-MS, thus indicating that the iron oxides in the sample Fe3-MS are better dispersed on the silica support, as also evidenced by TEM images and Mössbauer spectroscopy. It is interesting because these accessible iron oxides nanoparticles may effectively participate in the H_2O_2 activation processes to produce reactive species to catalytically oxidize organic compounds in water.

The EPR spectroscopy is a very sensitive technique for studying the nature and the crystal symmetry environment of iron in mesoporous silica. We, therefore, have carried out EPR measurements in the samples Fe2-MS and Fe3-MS. The signal at $g = 3.3$ and 2.9 in the Fe2-MS and Fe3-MS samples (Fig. 6), respectively, can be assigned to Fe^{3+} oxides, such as hematite and/or maghemite on the silica support. The incipient signal at $g \approx 2$ could be assigned to tetrahedrally coordinated Fe in the silica framework. However, for framework substituted iron usually two signals are present in mesoporous materials, namely $g \approx 2$ and $g \approx 4.3$, for symmetric and distorted environments. In the spectra of samples Fe2-MS and Fe3-MS only one of these two types is observed ($g \approx 2$), which is an indicative of that iron is practically present in the samples as hematite and maghemite.

The effect of iron precursor on the textural properties of prepared silica was evaluated by nitrogen physisorption (Fig. 7a). A dramatic change in the isotherms due to the use of different iron precursors was observed. For sample MS, the N_2 adsorption isotherm corresponded to type IV, meaning that they exhibit uniform hexagonal mesoporous structure, as shown in TEM images. Samples Fe3-MS and Fe2-MS also presented a type IV isotherm, however, the slight capillary condensation step exhibited by these samples is typical of disordered silica gels. The iron precursor strongly affected the specific area of the prepared silica, which was found to be 1406, 1165 and 799 $m^2\ g^{-1}$ for the samples MS, Fe3-MS and Fe2-MS, respectively. Despite the iron precursor affecting the specific area, the pore size distribution (Fig. 7b) practically does not change, remaining in the range of 15–40 Å in both samples.

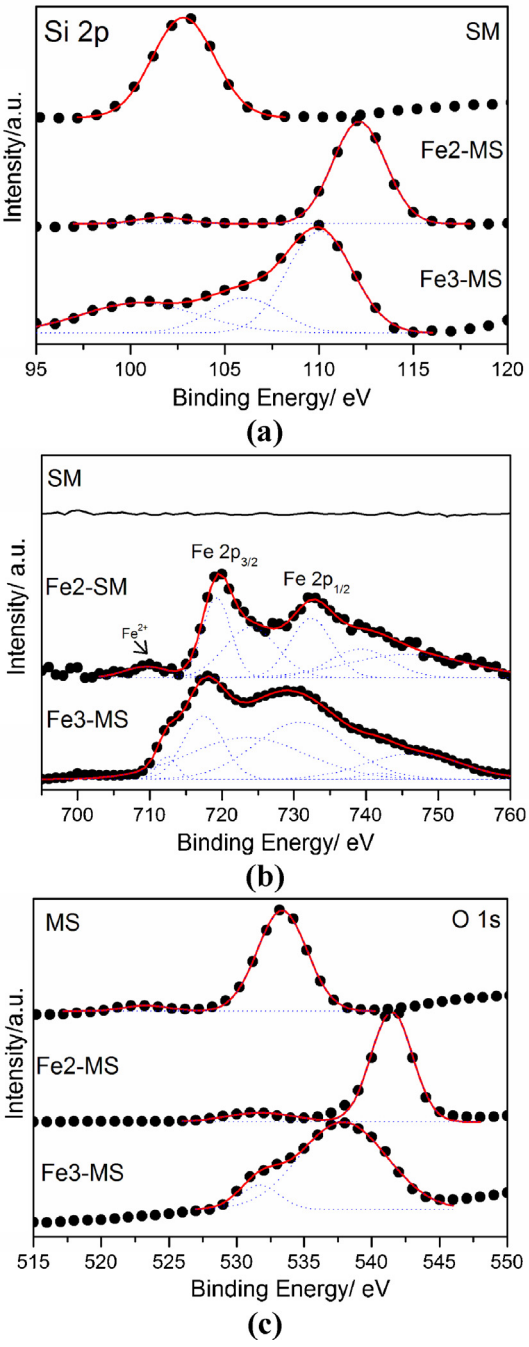

Fig. 4. XPS spectra of the MS, Fe2-MS and Fe3-MS samples: (a) Si 2p, (b) Fe 2p, (c) O 1s. Dotted lines – peaks used for the deconvolution of experimental spectrum.

3.2. Catalytic tests

Fig. 8 presented a comparison of the activities of the materials prepared to catalyze the methylene oxidation. In the absence of catalyst, the methylene blue dye (MB) oxidation was negligible up to 90 min reaction. On the other hand, in the presence of catalyst the removal capacity of methylene blue is significantly improved. In the first 20 min of reaction in the presence of MS, Fe2-MS and Fe3-MS were removed about of 4, 36 and 43%, respectively, from the 100 mg L^{-1} MB solution. After 90 min of reaction the removal was 19, 52 and 70% in the presence of MS, Fe2-MS and Fe3-MS, respectively. These results suggest that the iron is essential to produce an active Fenton-like system.

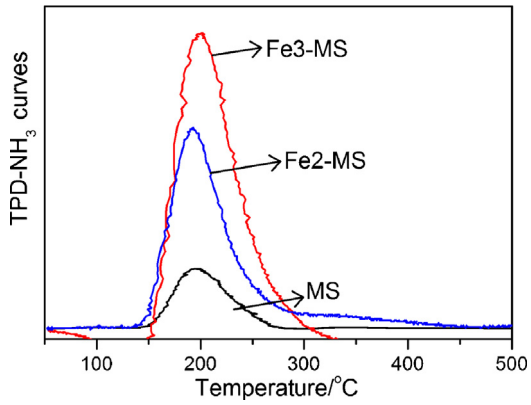

Fig. 5. TPD-NH_3 curves for the MS, Fe2-MS and Fe3-MS samples.

The Fe3-MS catalyst was found to be the most active to remove methylene blue because the Fe^{3+} oxides nanoparticles are better dispersed on the silica support and, therefore, they are more accessible to H_2O_2 activation. These smaller clusters of Fe^{3+} oxides embedded into the flexible pore walls of the mesoporous silica can efficiently participate in the reversible $Fe^{3+} \rightleftharpoons Fe^{2+}$ processes, which was essential to produce a more active Fenton-like system [31–37].

The point of zero charge (PZC) of the Fe2-MS and Fe3-MS samples (Fig. 9) was 0.2 and 1.0, respectively, suggesting that at pH 6 the silica particles are negatively charged, which can facilitate the cationic methylene blue adsorption on their surface. Thus, two processes should be considered to remove color from the methylene blue solution (i) adsorption of methylene blue on the silica particles and (ii) Fenton-like catalysis on the silica nanoparticles to produce colorless intermediates.

In order to prove the catalytic activity of Fe-containing silica particles rather than only adsorption on their surfaces, ESI-MS experiments were performed. Fig. 10 showed that after 60 min of reaction of methylene blue degradation in the presence of Fe2-SM and Fe3-SM several fragments of m/z = 270, 301, 318, 371 were produced, thus confirming that the catalytic activity takes place, rather than only adsorption on the catalyst surface. The fragment with m/z = 301 has been described as being due to hydroxylation in the methylene blue aromatic ring [38]. This is indirect evidence of the radical Fenton-like mechanism promoted by the Fe-containing mesoporous silica.

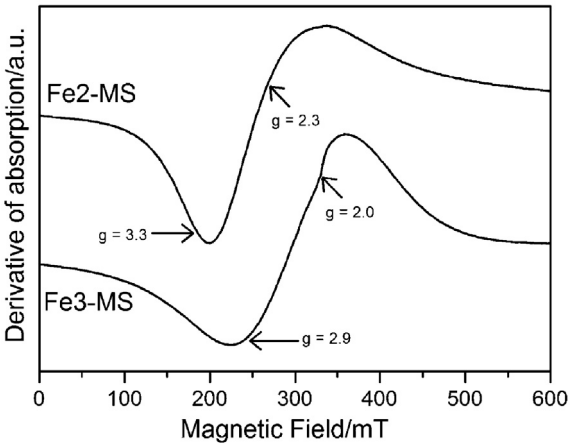

Fig. 6. EPR spectra for the MS, Fe2-MS and Fe3-MS samples.

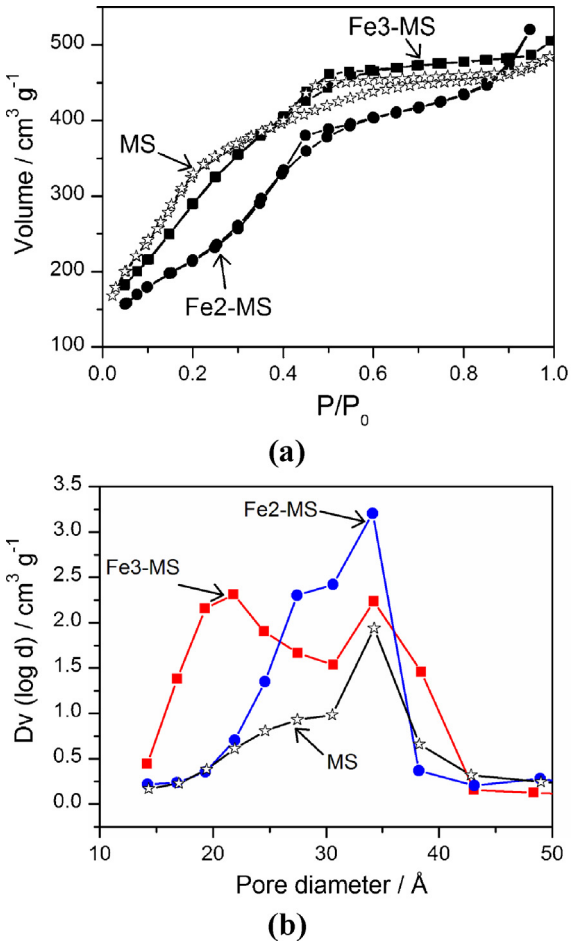

Fig. 7. (a) Nitrogen adsorption isotherms and (b) BJH pore size distributions of MS, Fe2-MS and Fe3-MS samples.

TG-MS profiles of Fe2-MS sample were collected after 60 min of methylene blue adsorption on its surface (Fig. 11a) and after the Fenton-like reaction (Fig. 11b). Comparing the profiles of thermal decomposition of the organic products on the Fe3-MS sample, it can be clearly observed that after the Fenton-like reaction the intermediate products exhibited fragments with smaller *m*/*z* ratio than in

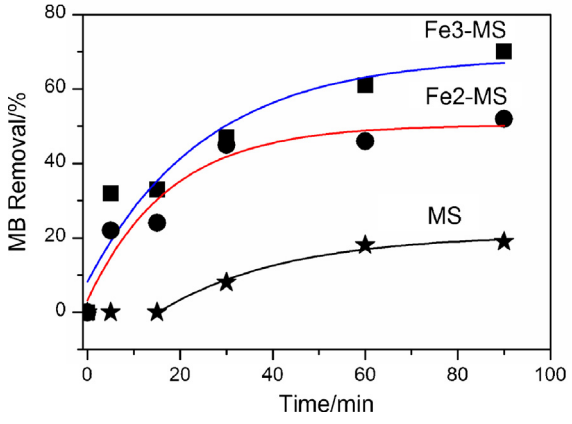

Fig. 8. Kinetic of methylene blue color removal in the presence of MS, Fe2-MS and Fe3-MS samples.

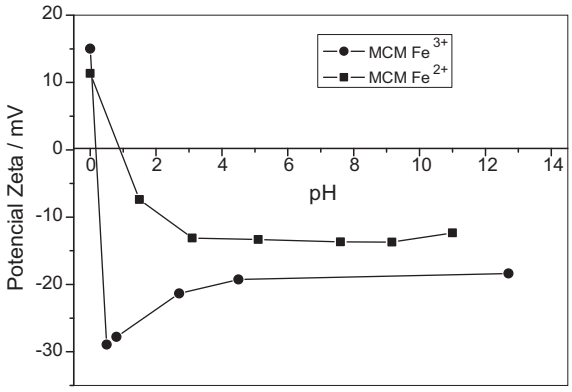

Fig. 9. Zeta potential measurements of MS, Fe2-MS and Fe3-MS samples as a function of pH.

the adsorption experiment. This is further evidence of the catalytic effect of the synthesized materials.

In order to evaluate if homogeneous reactions do occur, the catalysts were removed, by centrifugation, from the methylene blue aqueous solution after 60 min of reaction and the supernatants were monitored with UV–vis measurements after additional 24 h of reaction. The results suggested that 9 and 13% removal by Fe3-MS and Fe2-MS, respectively, were due to homogeneous reactions (Fig. 12). For effect of comparison, 5 wt.% hematite was impregnated on the MS sample and then catalytic tests were performed. After 60 min of reaction, the catalyst was removed from the reaction and the supernatant monitored to evaluate if a homogeneous reaction does occur. Thus, about 31% of color removal from methylene blue was due to homogeneous reactions. The higher homogeneous removal rate of silica impregnated with hematite suggests that the method used to prepare the catalysts in this work produced more stable materials toward Fe leaching. This was because the iron and silica matrix interaction is stronger if the iron precursor is added during the formation of silica gel, as verified by Mössbauer, XPS and EPR. The lower Fe leaching degree exhibited by the Fe3-SM sample was due to stronger interactions between the smaller clusters of Fe^{3+} oxides and the silica support. In view of this, the addition Fe in the course of silica synthesis is a promising alternative to produce efficient and relatively stable catalyst against Fe leaching to catalyze the oxidation of organics in water.

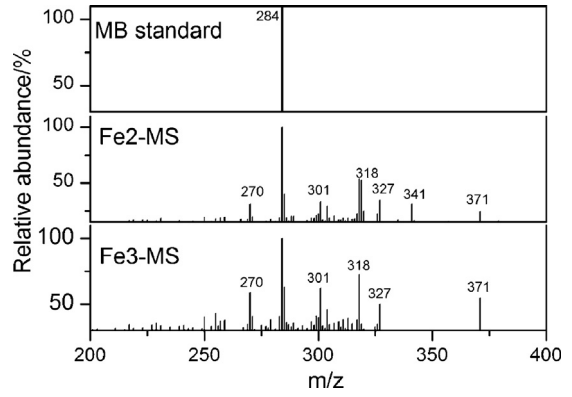

Fig. 10. ESI-(+)-MS of methylene blue and after 5 min of reaction in the presence of Fe2-MS or Fe3-MS.

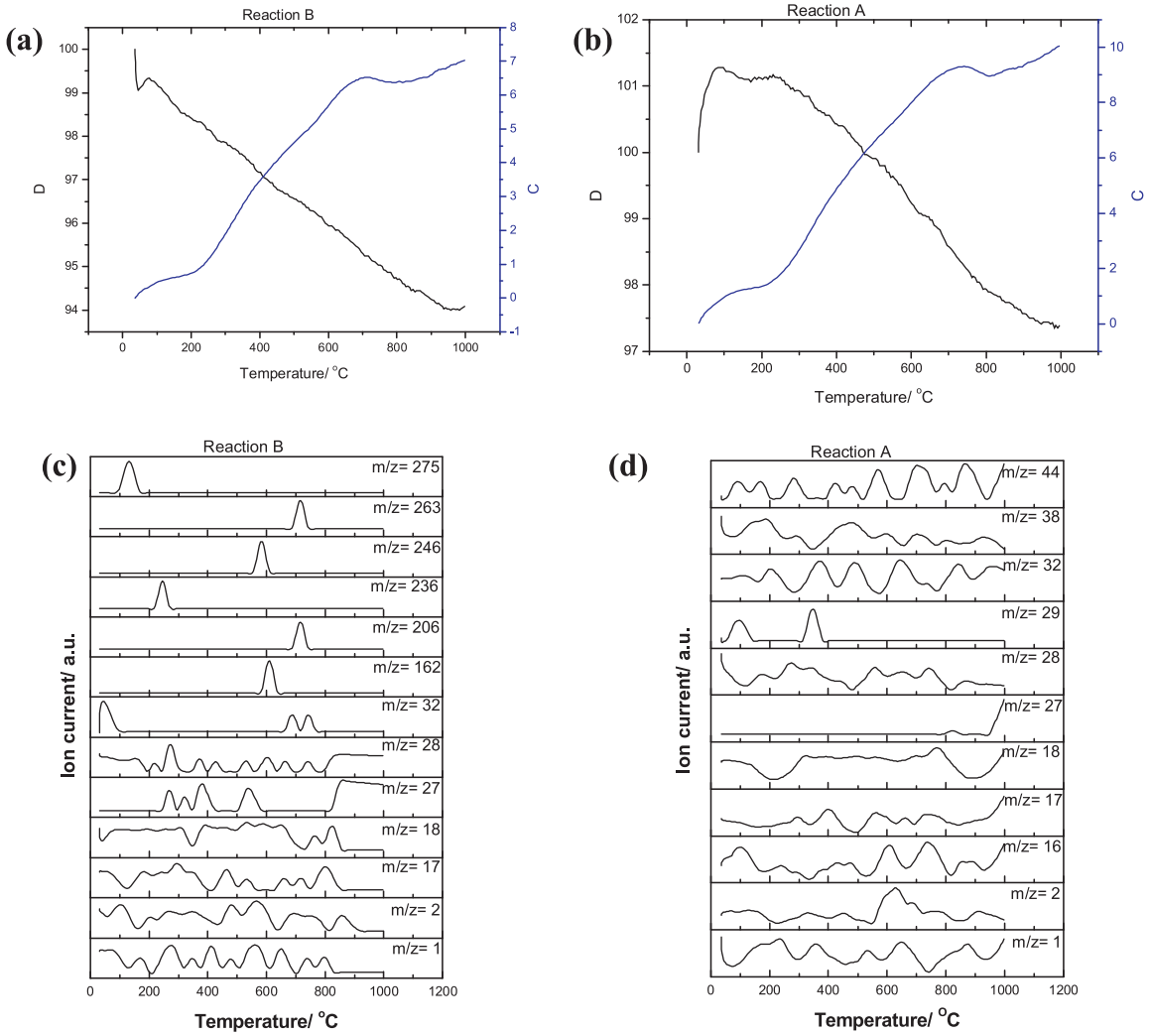

Fig. 11. TG-MS of (a and c) after 5 min of methylene adsorption on the Fe2-MS surface and (b and d) after 5 min of Fenton-like reaction in the presence of Fe2-MS.

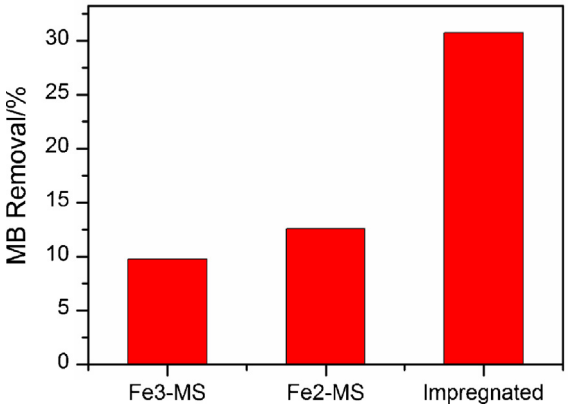

Fig. 12. Methylene blue color removal by homogeneous Fenton-like reactions in the presence of samples Fe2-MS, Fe3-MS and MS impregnated with 5 wt.% Fe_2O_3.

4. Conclusions

Fe_2O_3/mesoporous silica nanoparticles were prepared by adding Fe^{3+} or Fe^{2+} ions in the course of silica synthesis. The presence of these iron species during the synthesis strongly affected the ordered hexagonal arrays of silica. From low angle XRD, Mössbauer spectroscopy, XPS and EPR was evidenced that the iron in the samples Fe2-MS and Fe3-MS is due to a mixture of hematite and maghemite supported on the silica matrix. The Fe3-MS sample was found to be the most active Fenton-like catalyst to degrade methylene blue because the iron active sites are more exposed than the iron in the Fe2-MS sample. These smaller clusters of Fe^{3+} oxides embedded into the flexible pore walls of the mesoporous silica can efficiently participate in the reversible $Fe^{3+} \rightleftharpoons Fe^{2+}$ processes, which was essential to produce a more active Fenton-like system. A simple and cheap method was used to prepare an active Fenton-like catalyst by using Fe as precursor. These catalysts showed to be more active and stable against Fe leaching than that obtained by simple impregnation of iron on the silica matrix.

Acknowledgments

Financial support from the CNPq, CAPES, and FAPEMIG is gratefully acknowledged.

References

[1] M. Ziolek, P. Decyk, I. Sobczak, M. Trejda, J. Florek, H. Golinska, W. Klimas, A. Wojtaszek, Appl. Catal. A, Gen. 391 (2011) 194–204.
[2] D.Q.L. Oliveira, M. Gonçalves, L.C.A. Oliveira, L.R.G. Guilherme, J. Hazard. Mater. 151 (2008) 280–284.
[3] S.B.C. Pergher, L.C.A. Oliveira, A. Smaniotto, D.I. Petkowicz, Quim. Nova 28 (2005) 751–755.
[4] J.S. Beck, J.V. Vartuli, W.J. Roth, J. Am. Chem. Soc. 114 (1992) 10834–10843.

[5] C. García-Sancho, R. Moreno-Tost, J. Mérida-Robles, J. Santamaría-González, A. Jiménez-López, P. Maireles-Torres, Appl. Catal. A, Gen. (2012) 179–187, 433–434.
[6] F. Wang, Z. Shi, F. Hu, Z. Xia, L. Wang, Anal. Bioanal. Chem. 405 (2013) 1683–1693.
[7] M. Crişan, M. Răileanu, S. Preda, M. Zaharescu, A.M. Vălean, E.J. Popovici, V.S. Teodorescu, V. Matejec, J. Mrazek, J. Optoelectron, Adv. Mater. 8 (2006) 815–819.
[8] K. Szczodrowski, B. Prélot, S. Lantenois, J.M. Douillard, J. Zajac, Microporous Mesoporous Mater. 124 (2009) 84–93.
[9] C.R. Ringenbach, S.R. Livingston, D. Kumar, C.C. Landry, Chem. Mater. 17 (2005) 5580–5586.
[10] N. Pal, M. Paul, A.J. Bhaumik, Solid State Chem. 184 (2011) 1805–1812.
[11] M. Kanezashi, M. Asaeda, J. Membrane Sci 271 (2006) 86–93.
[12] F. Li, F. Xue, B. Chen, Z. Huang, Y. Yuan, G. Yuana, Appl. Catal. A, Gen. 449 (2012) 163–171.
[13] P. Decyk, M. Trejda, M. Ziolek, J. Kujawa, K. Głaszczka, M. Bettahar, S. Monteverdi, M. Mercy, J. Catal. 219 (2003) 146–155.
[14] A.C. Pradhan, B. Nanda, K.M. Parida, M. Das, Dalton Trans. 42 (2013) 558–566.
[15] D.S. Gopala, R.R. Bhattacharjee, R. Richards, Appl. Organomet. Chem. 27 (2013) 1–5.
[16] N. Marin-Astorga, J.J. Martinez, G. Borda, J. Cubillos, D.N. Suarez, H. Rojas, Top. Catal. 55 (2012) 620–624.
[17] G. Satishkumar, M.V. Landau, T. Buzaglo, L. Frimet, M. Ferentz, R. Vidruk, F. Wagner, Y. Gal, M. Herskowitz, Appl. Catal. B, Environ. 138–139 (2013) 276–284.
[18] Z. Lei, S. Bai, L. Dang, H. Xia, Q. Xu, Y. Cao, L. An, M. Zhao, A.Y. Lo, S.B. Liu, Microporous Mesoporous Mater. 123 (2009) 306–313.
[19] Y. Jiang, K. Lin, Y. Zhang, J. Liu, G. Li, J. Sun, X. Xu, Appl. Catal. A, Gen. 445–446 (2012) 172–179.
[20] J.V. Coelho, A.L.P. Meireles, K.A.S. Rocha, M.C. Pereira, L.C.A. Oliveira, E.V. Gusevskaya, Appl. Catal. A, Gen. 443–444 (2012) 125–132.
[21] N. Ferroudj, J. Nzimoto, A. Davidson, D. Talbot, E. Briot, V. Dupuis, A. Bée, M.S. Medjram, S. Abramson, Appl. Catal. B, Environ. 136–137 (2013) 9–18.
[22] R. Huang, B. Lan, Z. Chen, H. Yan, Q. Zhang, J. Bing, L. Li, Chem. Eng. J. 180 (2012) 19–24.
[23] D.Q. Khieu, D.T. Quang, T.D. Lam, N.H. Phu, J.H. Lee, J.S. Kim, J. Incl. Phenom. Macrocycl. Chem. 65 (2009) 73–81.
[24] M. Xia, C. Chen, M. Long, C. Chen, W. Cai, B. Zhou, Microporous Mesoporous Mater. 145 (2011) 217–223.
[25] J.S. Choi, S.S. Yoon, S.H. Jang, W.S. Ahn, Catal. Today 111 (2006) 280–287.
[26] S.V. Sirotin, I.F. Moskovskaya, B.V. Romanovcky, Catal. Sci. Technol. 1 (2011) 971–980.
[27] I. Ursachi, A. Stancu, A. Vasile, J. Colloid Interface Sci. 377 (2012) 184–190.
[28] F.L.Y. Lam, X. Hu, Catal. Commun. 8 (2007) 1719–1723.
[29] D. Jyothi, P.A. Deshpande, B.R. Venugopal, S. Chandrasekaran, G. Madras, J. Chem. Sci. 124 (2012) 385–393.
[30] A.C. Pradhan, K.M. Parida, J. Mater. Chem. 22 (2012) 7567–7579.
[31] L.C.A. Oliveira, J.D. Fabris, M.C. Pereira, Quim. Nova 36 (2013) 123–130.
[32] I.S.X. Pinto, P.H.V.V. Pacheco, J.V. Coelho, E. Lorençon, J.D. Ardisson, J.D. Fabris, P.P. de Souza, K.W.H. Krambrock, L.C.A. Oliveira, M.C. Pereira, Appl. Catal. B, Environ. 119–120 (2012) 175–182.
[33] M.C. Pereira, L.C.A. Oliveira, E. Murad, Clay Minerals 47 (2012) 285–302.
[34] M.C. Pereira, L.C.D. Cavalcante, F. Magalhães, J.D. Fabris, J.W. Stucki, L.C.A. Oliveira, E. Murad, Chem. Eng. J. 166 (2011) 962–969.
[35] M.C. Pereira, F.S. Coelho, C.C. Nascentes, J.D. Fabris, M.H. Araújo, K. Sapag, L.C.A. Oliveira, R.M. Lago, Chemosphere 81 (2010) 7–12.
[36] A.L. Andrade, D.M. Souza, M.C. Pereira, J.D. Fabris, R.Z. Domingues, J. Nanosci. Nanotechnol. 9 (2009) 3695–3699.
[37] M.C. Pereira, C.M. Tavares, J.D. Fabris, R.M. Lago, E. Murad, P.S.R. Criscuolo, Clay Minerals 42 (2007) 299–306.
[38] I.R. Guimaraes, A. Giroto, L.C.A. Oliveira, M.C. Guerreiro, D.Q. Lima, J.D. Fabris, Appl. Catal. B, Environ. 91 (2009) 581–586.